A.G.T. Cross
British Aerospace, Military Aircraft Division
Brough, N. Humberside, England

Abstract

This paper deals with the calculation of attached and separated flow using turbulent integral boundary layer theory, a law of the wall and wake form of velocity profile and a strong coupling equation based on the combined boundary layer and transpiration velocity equations.

Emphasis is placed on the velocity profile and the governing equations which are applicable to both two and three-dimensional flow.

I. Introduction

At the present time there is much interest in calculating the separated flow over aircraft wings in order to determine the all important buffet boundaries and maximum lift. So as to provide practical and fast design methods, the current trend is to match an inviscid calculation for the flow external to the shear layers with a boundary layer type calculation for the flow within the shear layers. This is the now classic viscous-inviscid coupling approach. However, when separated flow is involved this imposes particular difficulties not only on the coupling algorithm but also on the boundary layer method; which has to be able to handle flow reversal at the wall and in the wake. In this paper, it is shown that these difficulties can be overcome using formulations based on a modified form of the law of the wall and wake velocity profile, which allows for non-equilibrium flow distortion.

II. The Velocity Profile

Traditionally approximate forms of velocity profile, or an equivalent abstraction, have been used for integral boundary layer methods. Such approximations however, are a serious limitation if second order effects are to be included, or if three-dimensional flow is to be considered. In the latter case the additional integral thicknesses place greater emphasis on the precision of the velocity profile. All this, together with the requirement to handle separated flow, makes the law of the wall and wake particularly attractive for turbulent integral boundary layer calculation and this section of the present paper describes a modified form suitable for both two and three-dimensional calculations.

The profile can be extended to compressible flow, using the transformation of Spence[1], but in the interest of brevity only the incompressible form is described here.

Attached Flow

The law of the wall is derived from Prandtl's mixing length hypothesis, the assumption of constant shear stress close to the wall and by matching the law of the wall to the laminar sub layer. The wall flow is dominated by the wall shear stress with the skin friction coefficient becoming the primary independent variable. The matching of the wall flow with the laminar sub layer after suitable length and velocity scales, are specified results, as shown by Schlichting[2], in the Reynolds number dependence of the law of the wall. The wake region away from the wall is dominated, as may be expected, by the external flow inertia rather than wall friction and Coles[3] introduced a wake term with a weighting function related to the longitudinal or streamwise pressure gradient. The law of the wall and wake can be written as:-

$$\frac{Q}{Qe} = \frac{q}{K}\left[\mathrm{Ln}\left(\mathrm{Rd}\ q\ \frac{y}{d}\right) + A\right] + B\ \sin^{X}\left(\frac{\Pi}{2}\ \frac{y}{d}\right) \qquad (1)$$

With the Coles formulation the wake exponent X takes the value of 2 while the effect of pressure gradient is allowed for in the wake weighting function B. One of the prime disadvantages with the Coles formulation is that the velocity profile is not fully compatible at the outer edge of the boundary layer where it meets with the external inviscid flow. In order to include such a profile in an integral calculation method, it is essential to match the outer edge boundary condition Q = Qe at y=d and this requires that Coles weighting function reverts to a simple scale factor with a value given by:-

$$B = 1 - \frac{q}{K}\left[\mathrm{Ln}\ (\mathrm{Rd}\ q) + A\right] \qquad (2)$$

It is then necessary to reappraise the way in which pressure gradient is included and it was shown by Cross[4] that the wake exponent could be related to a departure from equilibrum flow through a relative pressure gradient parameter Πr. Thus, by consideration of the difference between the streamwise pressure gradient parameters of the actual flow and the equivalent equilibrium flow we have:-

$$X = F(\Pi r) \qquad (3)$$

where $$\Pi r = \left(\frac{\theta}{Qe}\ \frac{dQe}{ds}\right) - \left(\frac{\theta}{Qe}\ \frac{dQe}{ds}\right)_{EQ} \qquad (4)$$

Many studies have been made of turbulent boundary layers developing under conditions of equilibrium, or self preservation and it is found that they can be characterised by an equilibrium locus relating the shape parameter of the velocity defect profile to a pressure gradient parameter. The equilibrium locus can be used here to define the equilibrium term of Equation 4 and so complete the description of X. Very good results have been

*This work has been carried out with the support of Procurement Executive, Ministry of Defence

obtained using the locus proposed by Green et al[5], which after some rearrangement gives:-

$$\left(\frac{\theta}{Qe}\frac{dQe}{ds}\right)_{EQ} = \frac{1.25}{H}\left[\frac{Cf}{2} - \left(\frac{H-1}{6.432H}\right)^2\right] \quad (5)$$

Figure 1, is taken from Reference 4 and shows the correlation, with the relative pressure gradient parameter, of the values of X that give the optimum velocity profile fit to experimental data. It can be seen immediately from the figure that for equilibrium flow, that is $\Pi r = 0$, the Coles value still applies and so the velocity profile remains applicable to the wealth of data collected for equillibrium layers, for which the original law of the wall and wake is known to work well. However, for very strong pressure gradients values of X very different to the Coles value are required and this can be interpreted as a distortion of the profile related to the departure from equilibrium.

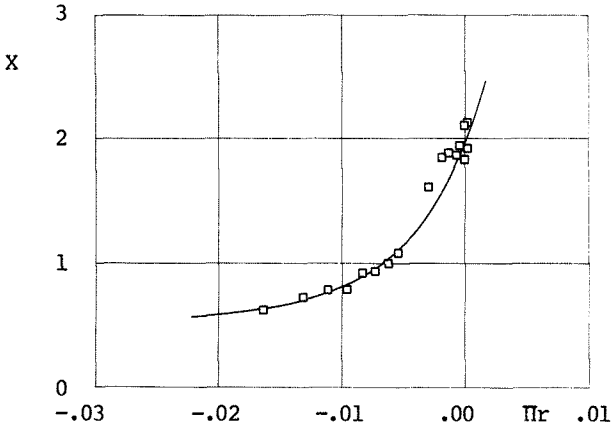

Figure 1. Non-equilibrium flow distortion for two-dimensional flow

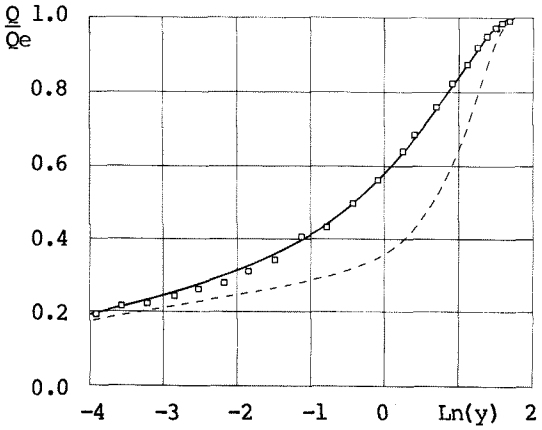

Figure 2. Velocity profiles; [] experiment, - - - - - - equilibrium flow theory, ——— general theory.

In order, to show the effect of this non-equilibrium distortion to the law of the wall and wake the experiment of East and Hoxy[6] is now considered. Figure 2 shows two theoretical velocity profiles compared with the experimental data; one profile for the Coles equilibrium value of X and one profile using the value determined from Figure 1. In both cases the measured skin friction coefficient and boundary layer thickness were used to construct the theoretical profiles and the effect of non-equilibrium flow distortion is clearly evident.

It is informative when considering velocity profiles for turbulent flow to examine the nature of the shape parameter relation Hl - H. The shape parameter Hl was introduced originally by Head[7] for entrainment type integral boundary layer calculation, while H is the more commonly known shape parameter. For the revised law of the wall and wake this shape parameter relation is a function of both Reynolds number and pressure gradient, with the former effect due to the wall flow and the latter due to that of the wake.

Figure 3 illustrates the effect on the shape parameter relation, of the law of the wall and wake, due to varying the Reynolds number at the equilibrium flow condition. The figure shows that the effects of Reynolds number are largely confined to low values of H. At the equilibrium flow condition, separation, as defined by zero skin friction, occurs with H = 4 and the figure shows the Reynolds number effect there to be negligible. This behaviour is explained by the logarithmic wall region vanishing at separation to leave only the wake term remaining.

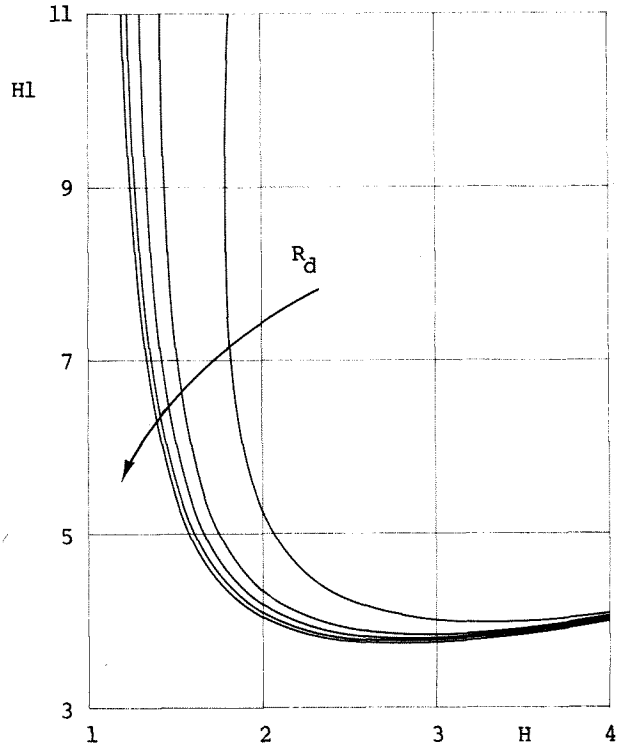

Figure 3. Shape parameter relation. Reynolds number variation for equilibrium flow; ——— Rd = 100, 1000, 10000, 1000000, infinity

An important consequence of the Reynolds number effect can be seen at the low values of H, where Reynolds number limits the minimum value of H attainable. This limit plays a very significant role in flow recovery due to a favourable pressure gradient and is amply demonstrated using the experiment of Chu and Young[8]. This experiment was for the flow over a flat plate with the suction

peak type pressure distribution shown in Figure 4. Figure 5 compares the experimental values of H with two entrainment integral method predictions; one using the modified law of the wall and wake and one using an empirical shape parameter relation in place of a velocity profile. The limit to the minimum value of H is clearly seen in the experiment and the law of the wall and wake calculation agrees very well with this. However, the calculation using the other method fails to predict this flow feature.

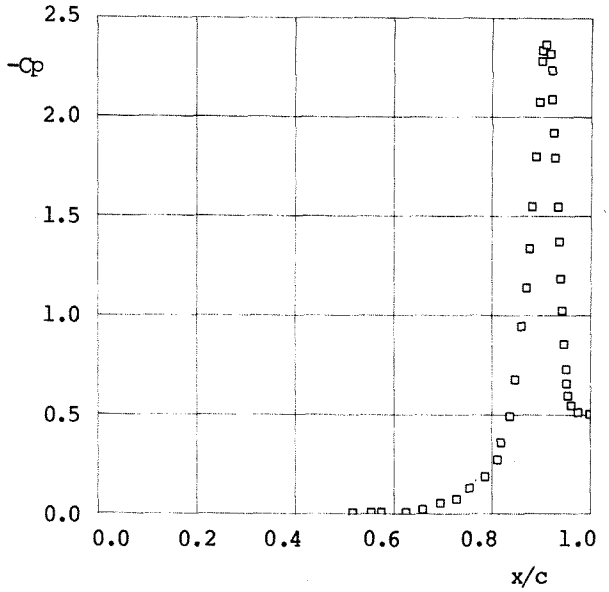

Figure 4. Pressure coefficient distribution; [] Chu and Young.

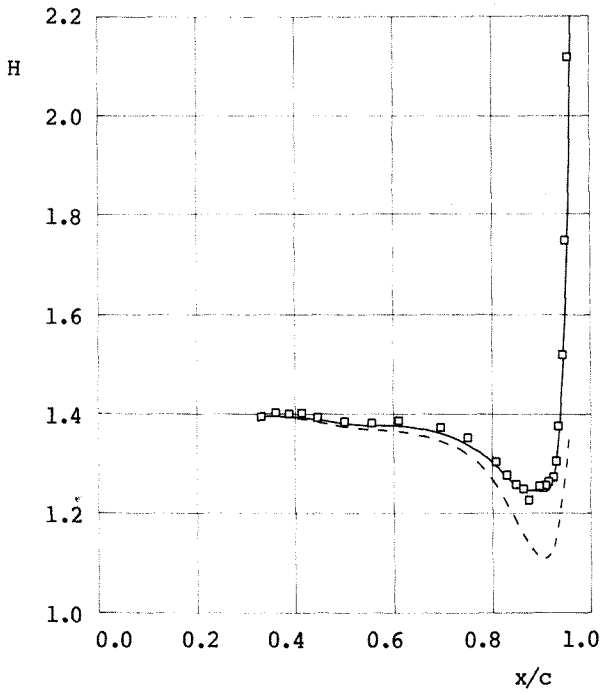

Figure 5. Shape parameter predicition; [] Chu and Young, ——— law of wall and wake method, - - - - - method of Green et al.

For non-equilibrium flow at constant Reynolds number, Figure 6 shows that the distortion of the shape parameter relation due to pressure gradient effects occurs mainly at high values of H and this is due to the dominance of the wake at these conditions. The main point to notice is that second order pressure gradient effects, that is those in addition to the direct effect in the boundary layer momentum equation, are likely to be important at separation.

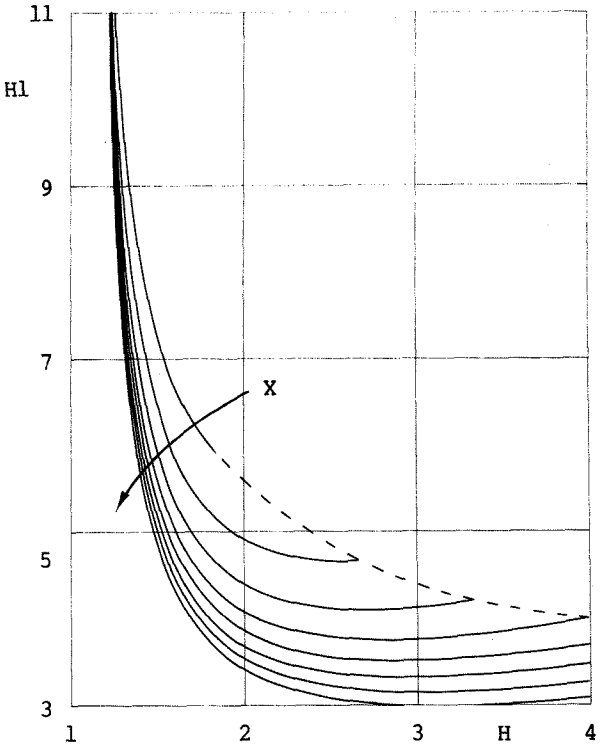

Figure 6. Shape parameter relation. Wake exponent variation at Reynolds number of 1 million; ——— X = .5 to 4, - - - - - zero skin friction locus.

Separated Flow

The law of the wall and wake can be applied to fully separated flow, though its original development was for attached flow with perhaps incipient separation. This extension is achieved by allowing the friction velocity to have negative values and so model flow reversal close to the wall. The first requirement is to avoid problems with the logarithmic term when the friction velocity goes negative and this is best achieved by writing the law of the wall and wake in the following form:-

$$\frac{Q}{Qe} = \frac{q}{K}\left[\frac{1}{2}\,\mathrm{Ln}\left(\mathrm{Rd}\,q\,\frac{y}{d}\right)^2 + A\right] + B\,\sin^{X}\left(\frac{\Pi}{2}\,\frac{y}{d}\right) \quad (6)$$

Figures 7 and 8 show the effect on the shape parameter relation when using the law of the wall and wake for separated flow. Figure 7 shows the influence of Reynolds number to be relatively small beyond separation in comparison to varying the relative pressure gradient parameter, and so wake exponent X as illustrated in Figure 8.

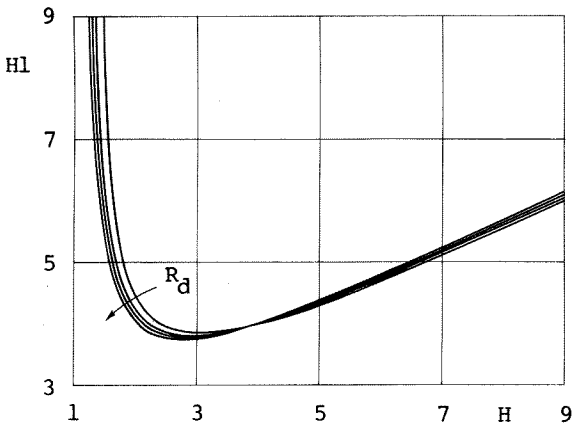

Figure 7. Extended shape parameter relation. Reynolds number variation for equilibrium flow; ——— Rd = 500, 5000, 50000, infinity.

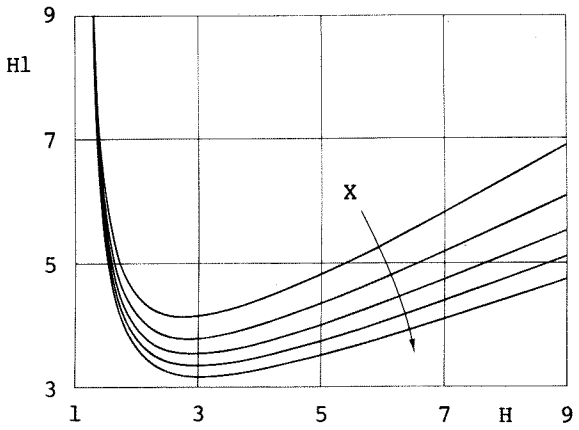

Figure 8. Extended shape parameter relation. Wake exponent variation at Reynolds number of 50000; ———— X = 1.5 to 3.5

Theoretical results are compared, in Figure 9, with the experimental data of Simpson et al[9]. The theoretical results are calculated for the appropriate experiment Reynolds number, using in one case the equilibrium value of wake exponent and in the other the values determined from the experimental values of pressure gradient and the correlation of Figure 1. The influence of the relative pressure gradient parameter is clearly evident beyond separation and produces the right effect, though the experiment suggests the effect ought to be stronger. Similar results are shown in Figure 10 for the experiment of Hastings and Williams[10]. This agreement is most encouraging, especially considering the velocity profile was developed originally for attached flow.

The results so far indicate a need for higher values of wake exponent at separation, than those given by Figure 1. Later, when three-dimensional flow is considered, it will become evident that at positive values of Πr, appropriate to fully developed separated flow, there is independent and direct evidence for revision of the correlation of Figure 1. This evidence, in the form of Figure 11, is consistent with the requirement for improved accuracy in the Figures 9 and 10. Further and just as important, the new evidence is not inconsistent with the two-dimensional data of Figure 1 as that was derived almost entirely from zero and negative values of the relative pressure gradient parameter.

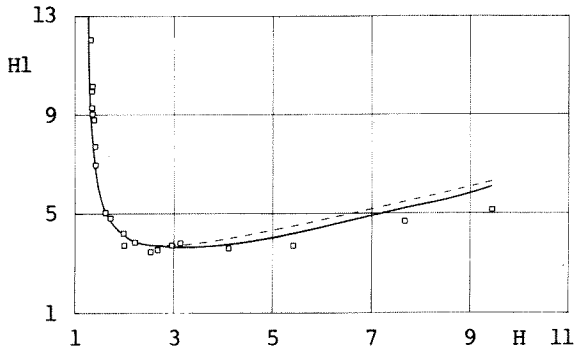

Figure 9. Extended Shape parameter relation; [] Simpson et al, - - - - - equilibrium flow theory, ———— general theory

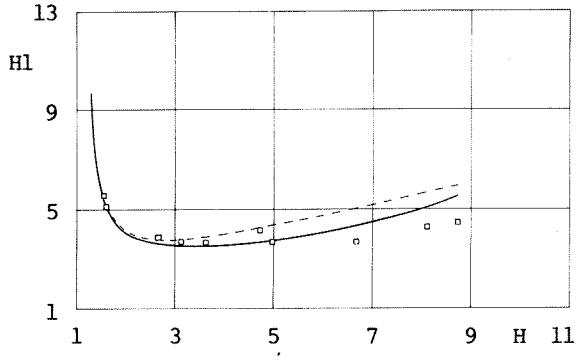

Figure 10. Extended Shape parameter relation; [] Hastings and Williams, - - - - - equilibrium flow theory, ———— general theory

Three-Dimensional Flow

The law of the wall can be extended to three-dimensions by considering the logarithmic wall region to lie in the direction of the surface streamline or so-called limiting streamline. This interpretation of a three-dimensional law of the wall is now quite widely recognised and can be verified by consideration of the experimental data of East and Hoxey[6] for highly three-dimensional flow and the data of Berg and Elsenaar[11] for sheared wing and plane flow. However, the law of the wake cannot be extended quite so easily into three-dimensions as it is twisted, or skewed throughout its thickness as was demonstrated in some detail in Reference 12.

As a first step towards extending the law of the wall and wake to three-dimensional flow, Equation 6 can be applied directly to the magnitude of the velocities in the three-dimensional turbulent boundary layer. This ignores the skewed nature of the wake but enables the effect of non-equilibrium flow distortion to be explored in exactly the same way as for the previously discussed two-dimensional case. Thus by analysing the data of East and Hoxey, together with that of Berg and Elsenaar, optimum values of the wake exponent for three-dimensional flow can be correlated against the departure from equilibrium. Figure 11 shows the results which are in good agreement with the original two-dimensional correlation of Figure 1.

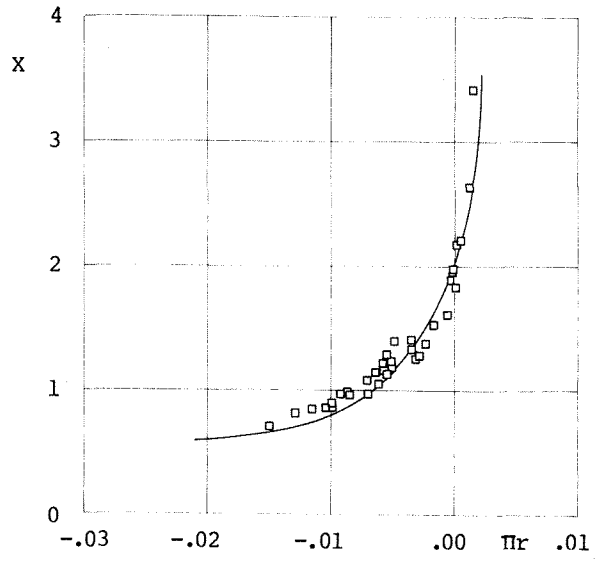

Figure 11. Non-equilibrium flow distortion for three dimensional flow.

To proceed further it is convenient to consider the three-dimensional form of the law of the wall and wake in streamline and crossflow components. The wall region simply resolves through the limiting streamline angle Bo, while in order to allow for a skewed wake separate streamwise and crossflow wake functions must be considered. Thus the profile can be written in the form:-

$$\frac{Qs}{Qe} = \frac{qs}{K}\left[\frac{1}{2}\,Ln\left(RD\ q\ \frac{y}{d}\right)^2 + A\right] + Bs\ \sin^{Xs}\left(\frac{\Pi}{2}\frac{y}{d}\right) \quad (7)$$

$$\frac{Qc}{Qe} = \frac{qc}{K}\left[\frac{1}{2}\,Ln\left(Rd\ q\ \frac{y}{d}\right)^2 + A\right] + Bc\ \sin^{Xc}\left(\frac{\Pi}{2}\frac{y}{d}\right) \quad (8)$$

where $qs = q\ \cos Bo$ (9)

$qc = q\ \sin Bo$ (10)

and where the wake exponents Xs and Xc are introduced to provide the necessary wake skewing. In addition, at the outer edge of the boundary layer, by definition of the streamline co-ordinate system we have:-

$$Qs = Qe,\ Qc = 0,\ y = d$$

and for the wake scale factors this requires:-

$$Bs = 1 - \frac{qs}{K}\left[\frac{1}{2}\,Ln(Rdq)^2 + A\right] \quad (11)$$

$$Bc = -\frac{qc}{K}\left[\frac{1}{2}\,Ln(Rdq)^2 + A\right] \quad (12)$$

We now consider the two wake functions. If the wake profile was not skewed it could be simply resolved, as for the wall flow, and this would effect the wake scale factors only so that we would have:-

$$Xs = Xc = X$$

However, the wake is skewed and the degree of twist can be expected to relate to the orientation of the wall and wake components of the velocity

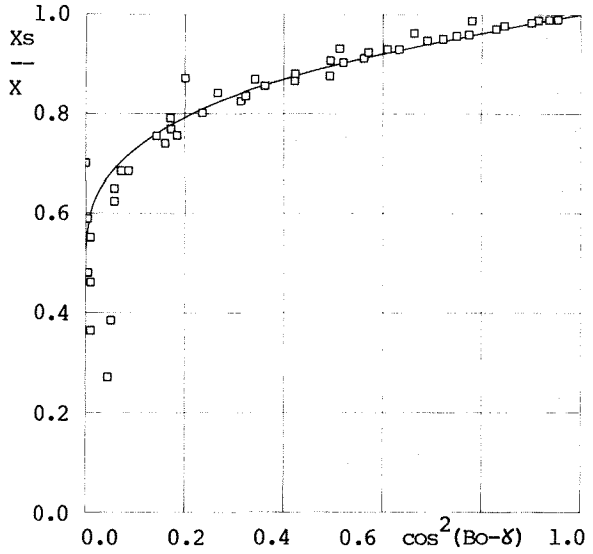

Figure 12. Streamwise wake exponent correlation, [] experiment, ——— correlation curve.

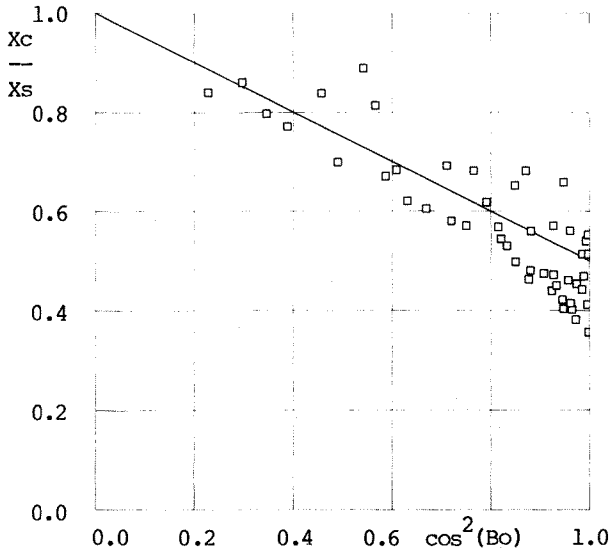

Figure 13. Crossflow wake exponent correlation, [] experiment, ——— correlation curve.

profile. The orientation of the wall region is of course given by Bo while that of the wake is determined by:-

$$\gamma = \tan^{-1}(Bc/Bs) \quad (13)$$

In addition to the orientation of the laws of the wall and wake, the wake exponents also relate directly to the exponent X of the previously determined scalar, or two-dimensional wake and so we anticipate correlations of the form:-

$$Xs = Xs\ (X,\ Bo,\ \gamma) \quad (14)$$
$$Xc = Xc\ (X,\ Bo,\ \gamma) \quad (15)$$

Any correlation should also be consistent with the two-dimensional form of velocity profile which when the flow is attached requires:-

$$Xs = X,\ Bo = 0,\ \gamma = 0$$

Whilst, two-dimensional separated flow requires:-

$$Xs = X,\ Bo = 180°, \gamma = 0$$

By further consideration of the experiments of References 6 and 11 correlations have been obtained for the wake exponents and these are shown in Figures 12 and 13.

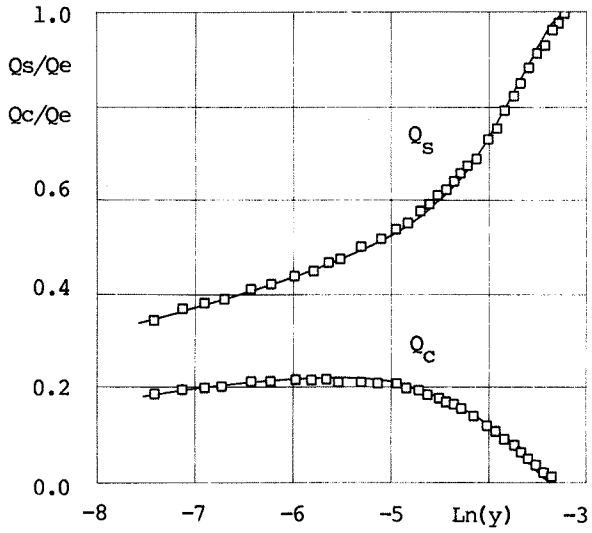

Figure 14. Theoretical velocity profiles compared with experiment; d = 40mm, Cf = .0017, Bo = 29.0 degrees; [] experiment, ——— theory.

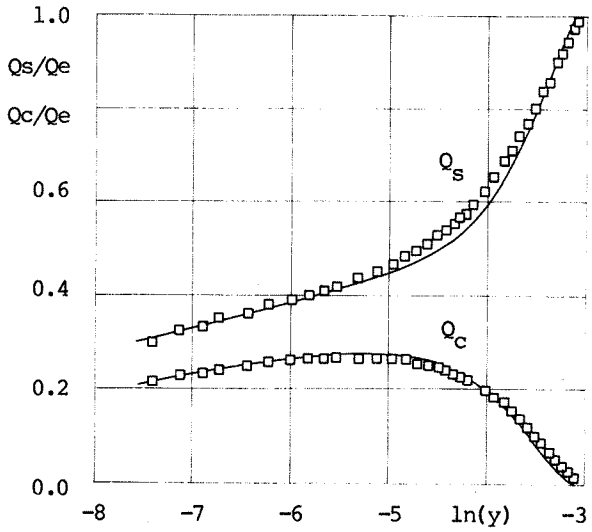

Figure 15. Theoretical velocity profiles compared with experiment; d = 48.5mm, Cf = .0015, Bo = 35.2 degrees; [] experiment, ——— theory.

Finally, Figures 14 and 15 show the results of fitting the three-dimensional law of the wall and wake profile to the experimental data of Berg and Elsenaar. The figures are for limiting streamline angles of 29 and 35.2 degrees respectively and the latter case is a particularly severe test as it was identified by Berg and Elsenaar as near the condition for a sheared wing form of separation. The main points to notice are that the streamwise flow components are similar to the two-dimensional velocity profile and that good agreement with experiment is obtained for both the streamwise and crossflow components.

Though the profile of Figure 15 is close to separation the value of the streamwise shape parameter is only 1.7 and the skin friction is far from zero. This illustrates the important difference between this type of separation and its two-dimensional counterpart. However the proposed velocity profile can model both these forms of separation.

III. The Coupling Equation

Starting with the three-dimensional boundary layer equations in streamline co-ordinates, as used by Myring[13] and more recently by Smith[14] for compressible flow, we may also add the equation[15] for the transpiration velocity, or Lighthill's equivalent source. The velocity profile is then introduced to produce a system of equations in terms of velocity profile parameters and the external stream velocities. By using the three-dimensional form of the law of the wall and wake these equations can be written in the following quasi-linear form:-

$$A_{ij} \frac{\partial Fj}{\partial s} + B_{ij} \frac{\partial Fj}{\partial n} = C_i + D_i \qquad (16)$$

where i = 1, 2, 3 and 4 refers to the entrainment, streamwise momentum, crossflow momentum and transpiration velocity equations respectively; where

$$F_1 = d,\ F_2 = qs,\ F_3 = qc,\ F_4 = \bar{Q}e.\ \bar{s}$$

$$C_1 = Ce,\ C_2 = q.\ qs,\ C_3 = q.\ qc,\ C_4 = \bar{Q}e.(\bar{s} \times \bar{n})$$

and where the coefficients D_i are the collected streamline curvature terms.

By combining the four equations, streamwise derivatives of boundary layer parameters can be eliminated and the result can be written in the following linearised form:-

$$a \frac{\partial}{\partial s}(\bar{Q}e.\ \bar{s}) + b \frac{\partial}{\partial n}(\bar{Q}e.\ \bar{s}) + c\ (\bar{Q}e.\ \bar{s}) = d\ \bar{Q}e.\ (\bar{s} \times \bar{n}) \qquad (17)$$

This equation can be seen to involve only the inviscid velocity external to the boundary layer and so can be interpreted as a viscous boundary condition for the external flow. Solutions of the boundary layer equations enable the coefficients of this equation to be calculated and as these vary much more slowly than either displacement thickness or transpiration velocity, then rapid convergence results for viscous-inviscid coupled flow solutions. For convenience, Equation 17 will be referred to as the strong coupling equation throughout the remainder of this paper.

When the external flow is irrotational the strong coupling equation can be further simplified using the irrotational flow equation, which for the streamline co-ordinate system can be written as:-

$$Kn\ (\bar{Q}e.\bar{s}) = \frac{\partial}{\partial n}(\bar{Q}e.\bar{s}) \qquad (18)$$

IV. Calculations

The velocity profile, boundary layer equations and strong coupling equation previously described have been used to provide the viscous routines for two and three-dimensional viscous flow methods. This viscous package has been used in conjunction with Petrie's[16] three-dimensional subcritical panel method, its two-dimensional equivalent and with Sinclair's[17] two-dimensional field panel method for solution to the full potential equation.

The calculations presented in this paper are for the two dimensional panel method which has been used to explore the convergence properties of the strong coupling equation. The calculations include wake relaxation and wake displacement effects but do not include normal pressure gradient terms, or indeed wake curvature, other than that obviously implied by wake relaxation.

The test case chosen was the NACA 4412 aerofoil of Williams and Hastings[10]. This test case is particularly useful as Williams provides a known target for computational methods following the calculations performed using his semi-inverse method.

In order to provide a critical test of the viscous method, the aerofoil section has been modelled with a sharp trailing edge and no smoothing, or other manipulation of data, has been introduced at the trailing edge, or indeed anywhere else in the flow. Thus calculations presented represent genuine solutions to the coupling problem with errors associated only with the validity of the mathematical model and the discrete treatment of the geometry involved.

Basic calculations involving the panel method were performed using a 60 point cosine distribution of control points on the aerofoil and a half cosine distribution of 30 control points in the wake. The wake extended a full chord distance downstream of the trailing edge with comparable control point spacing on the aerofoil and wake in the trailing edge region. In addition the calculations were performed allowing for the presence of a solid wall wind tunnel so that comparisons could be made with uncorrected wind tunnel data. Such comparisons are desirable as they are free of any dependence on wind tunnel corrections which are particularly uncertain at high lift.

Transition was fixed in the calculations at the nearest control points to the actual trip positions used in the experiment. Further, in accordance with the findings of Williams, a nominal jump in momentum thickness of .0002m was used at the upper surface trip to simulate the effect of a very coarse tripping device.

In order to demonstrate convergence, the lift coefficient and the trailing edge values of the boundary layer shape parameter have been recorded at each iteration of the calculations. As a further more critical guide to convergence the maximum external flow velocity change, E, between successive iterations has also been recorded. This quantity is particularly useful as its logarithm gives a direct measure of the order of accuracy.

In addition to the basic calculations the effect of a doubling of the number of control points has been demonstrated. Finally, calculations are shown for the separated flow conditions appropriate to the experiment and a comparison made between experiment and theoretical results.

Convergence of solutions

Preliminary calculations showed that the method could produce solutions in the absence of any use of relaxation factors. In some cases, over-relaxation could be used to accelerate convergence and for these cases the relaxation was applied to the singularity strengths, or the velocities calculated by the panel method. A degree of under-relaxation was sometimes necessary during the first three or four iterations, when changes were most rapid. However the degree of under-relaxation, required during the early iterations, was not very significant and a relaxation factor of 0.9 overcame any difficulties.

Convergence has been examined at 8, 10 and 12 degrees of incidence. Figures 16, 17 and 18 show the effects on convergence of calculations at 8 degrees of incidence. The figures show a regular convergence after the initial few iterations and four figure accuracy was obtained after 12 iterations.

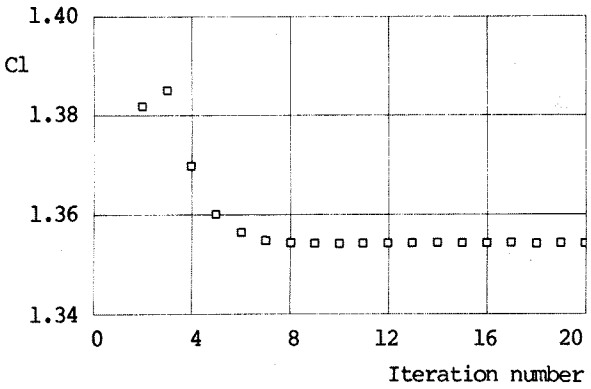

Figure 16. Convergence history of lift coefficient. Calculations at incidence 8° and Reynolds number 4170000.

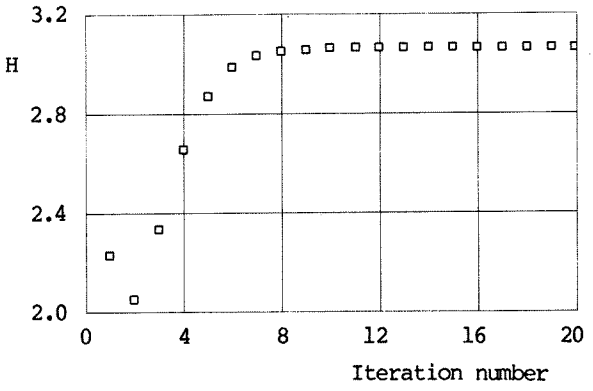

Figure 17. Convergence history of shape parameter. Calculations at incidence 8° Reynolds number 4170000.

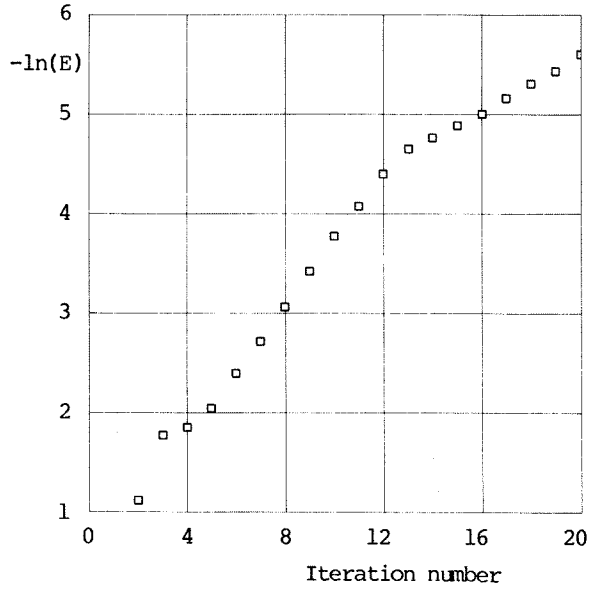

Figure 18. Convergence rate of the external flow velocities. Calculations at Incidence 8°, Reynolds number 4170000.

For the next part of the investigation it was decided to examine the effect of doubling the numbers of control points used to represent the aerofoil and wake and so refine the solution. For the Carter[18] and Balleur[19] type of coupling scheme this would normally require a large reduction in the under-relaxation parameter of the coupling equation with an increase in the number of iterations to achieve convergence. In addition to the computation refinement the calculations for this exercise were performed at a more critical incidence of 10 degrees. Two calculations were produced with one using the original geometry and one with the refined geometry. In every other respect the calculations were identical.

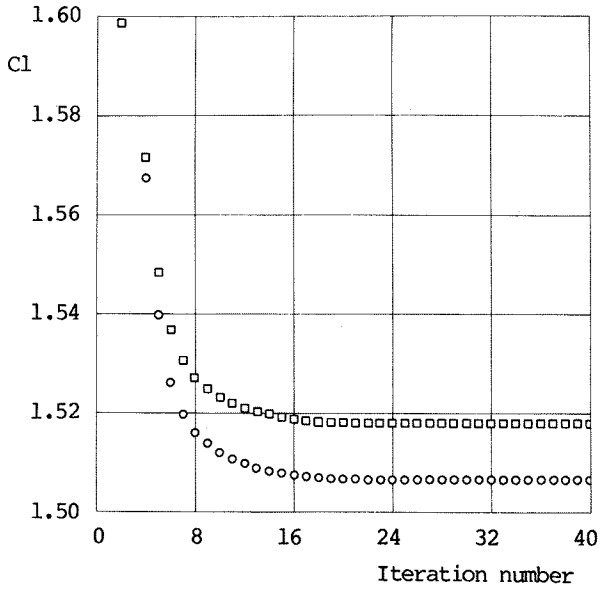

Figure 19. Convergence history of lift coefficient. Calculations at incidence 10° and Reynolds number 4170000; [] coarse geometry, O refined geometry.

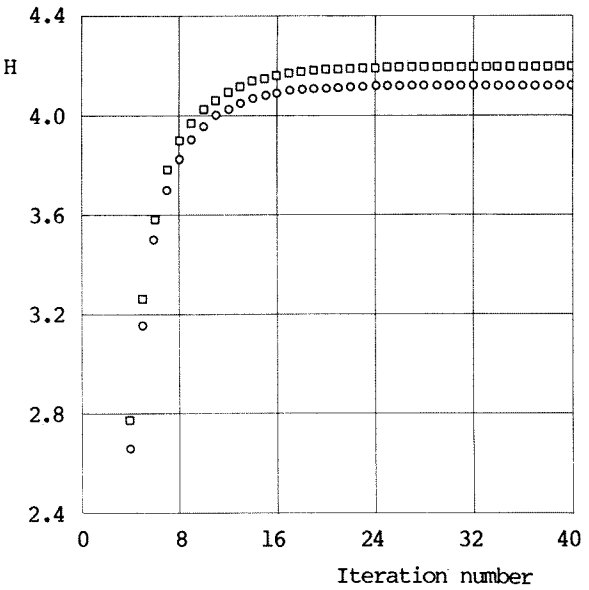

Figure 20. Convergence history of shape parameter. Calculations at incidence 10°, Reynolds number 4170000; [] coarse geometry, O refined geometry.

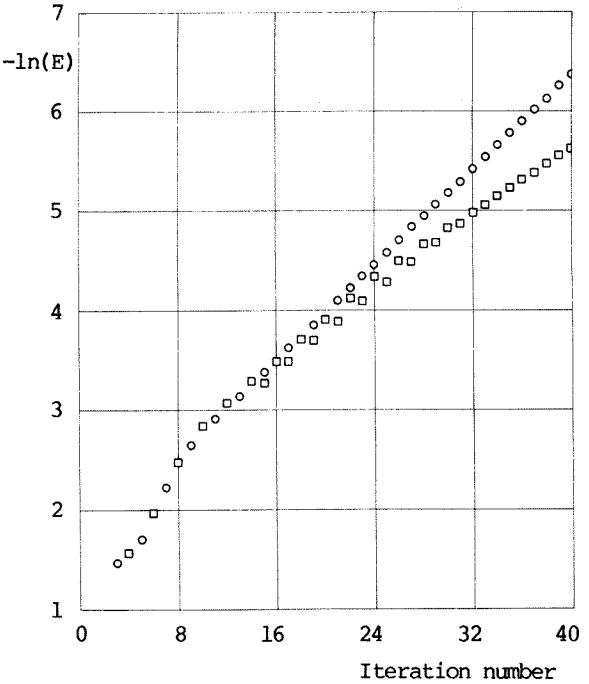

Figure 21. Convergence rate of the external flow velocities. Calculations at Incidence 10°, Reynolds number 4170000; [] coarse geometry, O refined geometry.

The results of the calculations are shown in Figures 19, 20 and 21. The refined calculation not surprisingly converges to a different solution to that of the calculation using the original goemetry but this difference is somewhat larger than would normally be expected. The difference was investigated and traced to slight differences in the transition position due to transition being fixed at the nearest control point to the actual

trip position used in the experiment. Together with the required momentum thickness jump at transition, this shows that for high lift cases solutions are quite sensitive to the conditions at transition.

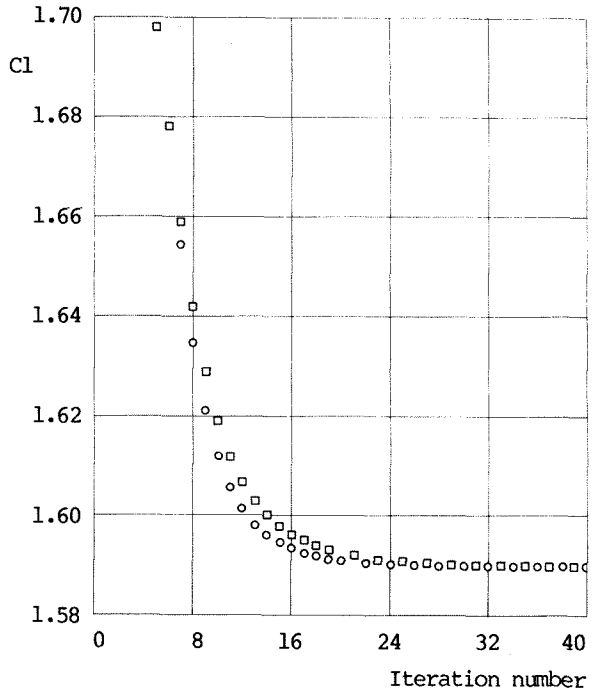

Figure 22. Convergence history of lift coefficient. Calculations at incidence 12° and Reynolds number 4170000; [] relaxation factor 0.9, O relaxation factor 1.1.

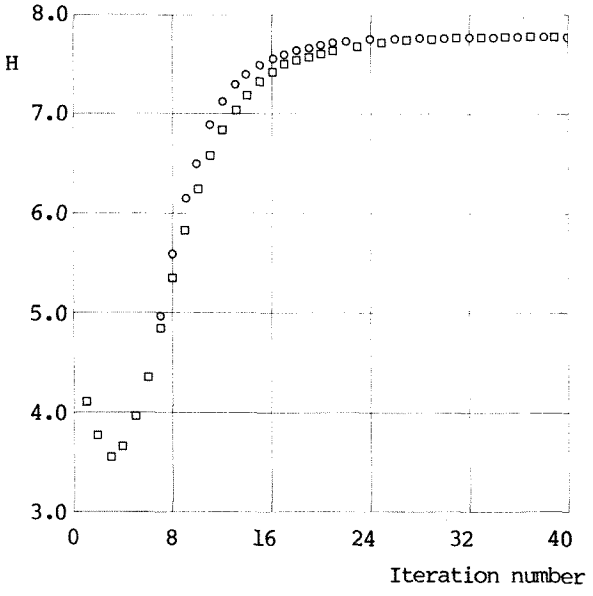

Figure 23. Convergence history of shape parameter. Calculations at incidence 12° Reynolds number 4170000; [] relaxation factor 0.9, O relaxation factor 1.1.

The crude and refined solutions both converge at similar rates but are slower to converge than the 8 degree incidence case previously shown. This time the calculations indicate 20 iterations to achieve an accuracy of four significant figures. Surprisingly the refined solution converges at a slightly better rate and in a more regular fashion than the crude solution.

As a final test of convergence behaviour, further calculations using the refined geometry have been undertaken at 12 degrees of incidence.

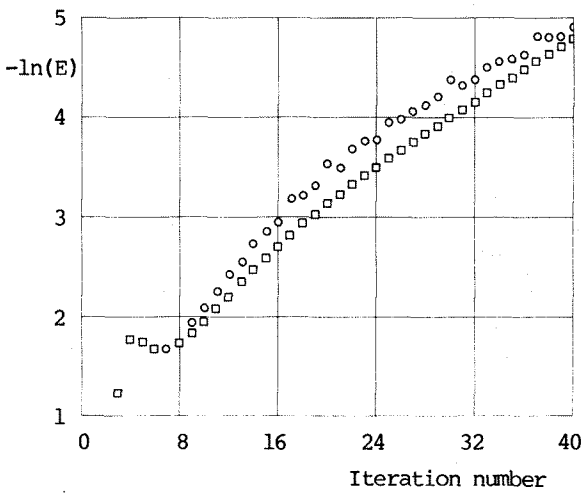

Figure 24. Convergence rate of the external flow velocities. Calculations at Incidence 12°, Reynolds number 4170000; [] relaxation factor 0.9, O relaxation factor 1.1.

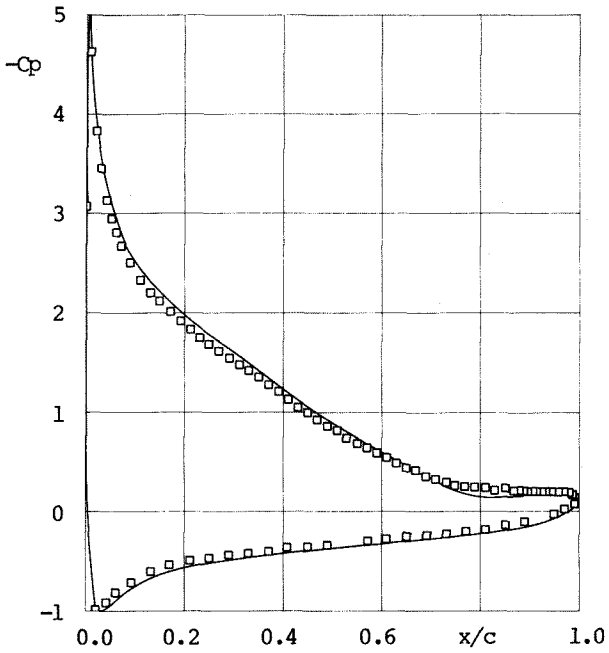

Figure 25. Pressure coefficient distributions; NACA 4412 aerofoil, incidence 12.25°, Reynolds number 4170000; [] experiment, ——— theory.

Figures 22, 23 and 24 show the results of this exercise. For one calculation the default relaxation factor of 0.9 was used while in a second calculation a relaxation factor of 1.1 was used from the fifth iteration onwards. The results show that over-relaxation does in fact improve convergence rate with four figure accuracy being

obtained after 26 iterations as opposed to 30 iterations using under-relaxation.

Comparison with experiment

Now we turn our attention to the particular incidence case for which Williams and Hastings report measurements. This was at an incidence of 12.25 degrees at a Reynolds number of 4.17 Million and at a Mach number of 0.176. Figure 25 shows the calculation results, in terms of pressure coefficient distribution, compared with experiment. As the calculation includes the effects of the tunnel walls the experimental data has been left in its uncorrected form and there are no worries about the uncertainties of tunnel corrections. The results are thought to be in reasonable agreement considering that normal pressure gradient and wake curvature effects have not been included at this stage.

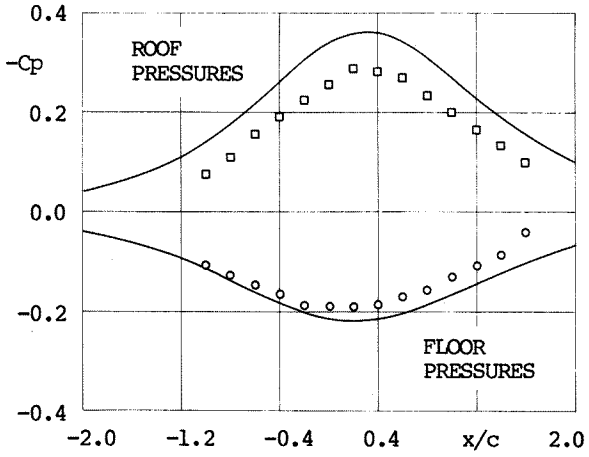

Figure 26. Tunnel wall Pressure coefficients; NACA 4412 section, incidence 12.25°, Reynolds number 4170000, tunnel height 2.74m, model height 1.37m; [], 0 experiment, ——— theory.

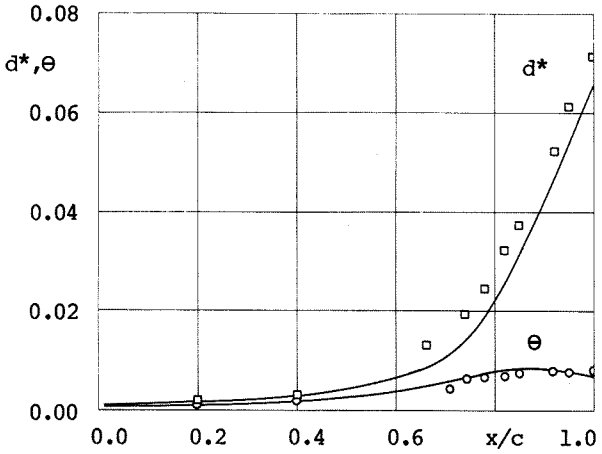

Figure 27. Integral thicknesses; NACA 4412 section, incidence 12.25°, Reynolds number 4170000; [], O experiment, ——— theory.

Figure 26 compares the calculated pressures with experimental data for the tunnel roof and floor. The main points to notice are that the shape of the two distributions are very similar but that they differ in magnitude with the calculated results suggesting the stronger wind tunnel interference and blockage effect. The results are consistent with the increased lift of the calculation that can readily be inferred from Figure 25. Figure 27 shows the boundary layer integral thicknesses for the upper surface of the aerofoil compared with the experimental data. The main difference is in the displacement thickness that consistently under estimates the experiment throughout the calculation. Part of this may be due to normal pressure gradient effects in the boundary layer.

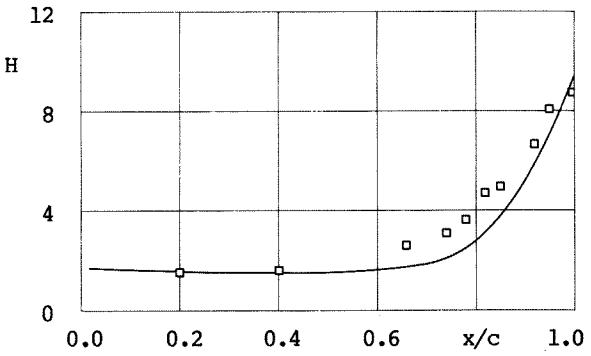

Figure 28. Shape parameter; NACA 4412 section, incidence 12.25°, Reynolds number 4170000, [] experiment, ——— theory.

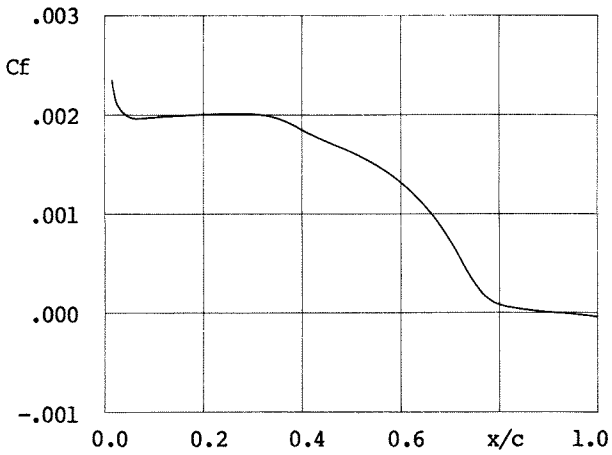

Figure 29. Skin friction coefficient; NACA 4412 section, incidence 12.25° Reynolds number 4170000; ——— theory.

Finally Figures 28 and 29 show the shape parameter and the skin friction coefficient for the upper surface of the aerofoil. The shape parameter is in broad agreement with experiment and otherwise unremarkable but the distribution of skin friction coefficient is particularly interesting as after an initial rapid fall the values flatten out to produce a gradual creep through the separation point. In the experiment separation was found to occur at about the 80% chord position while the calculation shows separation, based on zero skin friction, to occur at the 90% chord position. However, the skin friction creep associated with separation starts near the 80% chord position and this agrees with the start of the separated 'pressure plateau' region in the pressure distribution; the words 'pressure plateau' are used here somewhat loosely as the pressures show a slight dip at separation when plotted to the scale as used in Figure 25.

V. Conclusions

A modified form of the law of the wall and wake is presented for three-dimensional turbulent attached and separated flow. It is also shown that by combining the boundary layer equations with the transpiration velocity equation that a so-called strong coupling equation can be produced for viscous-inviscid interactions.

Solutions to the strong coupling equation have been demonstrated for a two-dimensional aerofoil using a subcritical panel method and a lag entrainment boundary layer method based on the modified law of the wall and wake. Solutions converge rapidly without the need for smoothing or other manipulation of data in strong interaction regions. Doubling the numbers of control points used to define the aerofoil and wake results in a slight improvement in convergence rate and this is a complete reversal of the trend associated with Carter and Balleur type coupling Schemes.

Over-relaxation of the external flow velocities can be used to speed convergence as can using initial conditions appropriate to previous lower incidence solutions.

Results have been compared with experiment for the NACA 4412 separated flow aerofoil test case of Hastings and Williams. The calculations include the presence of the tunnel walls and so direct comparison has been possible with uncorrected wind tunnel data. This is important as the standard wind tunnel corrections are in some doubt at high lift. The agreement with experiment is considered quite good considering that important second order effects are not included at this stage.

VI. List of Symbols

A Law of the wall constant
B Wake scale factor
c Reference length - aerofoil section chord
Ce Entrainment coefficient
Cf Skin friction coefficient
E Error parameter: maximum velocity change between successive iterations
H Shape parameter
Hl Head's shape parameter - $(d - d^*)/\theta$
K Prandtl's mixing length proportionality constant
Kn Streamline curvature
$\underline{n}$ Cross flow displacement
$\overline{n}$ Cross flow unit displacement vector
q Non-dimensional friction velocity
Q Streamwise Velocity
Rd Reynolds number based on boundary layer thickness
$\underline{s}$ Streamwise displacement
$\overline{s}$ Streamwise unit displacement vector
x Chordwise displacement
y Normal to wall distance
Bo Limiting streamline angle
γ Wake orientation angle
d Boundary layer thickness
d* Boundary layer displacement thickness
θ Boundary layer momentum thickness
Πr Relative pressure gradient parameter
X Wake exponent

In addition to the above symbols, the suffix (e) is used to denote values at the outer edge of the boundary layer while the suffix (EQ) is used to denote equilibrium values. Further, for three-dimensional flow the suffices (s) and (c) are used respectively for streamwise and crossflow components of variables.

VII. References

[1] Spence, D.A. The growth of compressible turbulent boundary layers on isothermal and adiabatic walls. ARC R. & M. 3191, 1961.

[2] Schlichting, H. Boundary layer theory. English edition, Pergamon Press, 1955.

[3] Editors: Kline, S.J. et al. Computation of turbulent boundary layers. AFOSR-IFP Stanford Conference Proceedings, 1968.

[4] Cross, A.G.T. Boundary layer calculations using a three parameter velocity profile. British Aerospace (Brough) Report YAD 3428, 1980.

[5] Green, J.E. Weeks, D.J. and Brooman, J.W.F. Prediction of turbulent Boundary layers and wakes in compressible flow by a lag entrainent method. RAE TR 72231, 1973.

[6] East, L.F. and Hoxey, R.P. Low speed three dimensional turbulent boundary layer data. ARC R. & M. 3653, 1969.

[7] Head, M.R. Entrainment in the turbulent boundary layer. ARC R. & M 3152, 1958.

[8] Chu, J.K. and Young, A.D. Measurements in separating two-dimensional turbulent boundary layers. AGARD CP 168, 1975.

[9] Simpson, R.L. Chew, Y.T. and Shivaprasad, B.G. The structure of a separating turbulent boundary layer: Part 1. mean flow and Reynolds stresses. J. Fluid Mech. Vol 113, 1981.

[10] Hastings, R.C. and Williams, B.R. Studies of the flow field near a NACA 4412 aerofoil at nearly maximum lift. RAE TM AERO 2026, 1984.

[11] Van den Berg, B. and Elsenaar, A. Measurements in a three-dimensional incompressible turbulent boundary layer in an adverse pressure gradient under infinite swept wing conditions. NLR TR 72092U, 1972.

[12] Cross, A.G.T. A means of closure for Coleman's three-dimensional turbulent boundary layer integral method. British Aerospace (Brough) Report YAD 3289, 1976.

[13] Myring, D.F. An integral prediction method for three-dimensional turbulent boundary layers in incompressible flow. RAE TR 70147 1970.

[14] Smith, P.D. Direct and inverse integral calculation methods for three-dimensional turbulent boundary layers. J. Royal Aero. Soc. May 1984

[15] Lighthill, M.J. On displacement thickness. J. Fluid Mech. Vol. 4, 1958

[16] Petrie, J.A.H. Development of an efficient and versatile panel method for aerodynamic problems. Leeds University Ph.D. thesis, 1979.

[17] Petrie, J.A.H. and Sinclair, P.M. Application and developments of computational methods for the aerodynamic problems of complex configurations. AGARD FDP Symposium, Aix-En-Provence, 1986.

[18] Carter. J.E. A new boundary layer inviscid iteration technique for separated flows. AIAA Paper 79-1450. 1979

[19] Le Balleur, J.C. Strong matching method for computing transonic viscous flows including wakes and separations: lifting aerofoils. La Recherche Aerospatiale 1981-3, 1981.